Blockade of Receptor for Advanced Glycation End Products in a Model of Type 1 Diabetic Leukoencephalopathy

Natalia Rincon,[1] Kevin Xu,[1] Jemma Li,[1] Jose A. Martinez,[1] Monica A. Hernandez,[1] Geeta S. Singh,[1] David Han,[1] Paul Lalli,[1] Amit Ayer,[1] Kevin Tse,[1] LingLing Rong,[2] Ann Marie Schmidt,[2] and Cory C. Toth[1]

Humans with type 1 diabetes mellitus (DM) are subject to the development of diabetic leukoencephalopathy (DLE) with cognitive decline, brain atrophy, and white matter abnormalities. We examined advanced glycation end products (AGE) and upregulation of their receptor (RAGE) stimulated by persistent hyperglycemia as a causative pathway, intervening with RAGE blockade in a murine DLE model of type 1 (streptozotocin) DM. Over 8 months, DM mice received intraperitoneal injections of soluble RAGE or placebo alongside non-DM mice and $RAGE^{-/-}$ mice. Cognitive testing and magnetic resonance imaging (T2, magnetization transfer, diffusion tensor imaging), neuronal and oligodendroglial counts, synaptic and myelin measures, and RAGE–nuclear factor (NF)-κB pathway assessment was performed serially. DM mice developed cognitive deficits after 8 to 20 weeks of DM, oligodendroglial loss after 3 months, brain atrophy after 5 months, loss of synaptic machinery and fractional anisotropy at 8 months, and RAGE–NF-κB pathway activation. DM mice receiving soluble RAGE and $RAGE^{-/-}$ DM mice were protected from most of these abnormalities. Although DM led to NF-κB upregulation, NF-κB–mediated gene transcription was downregulated at 8 months, possibly due to later upregulation of transcription repressors B-cell lymphoma 3-encoded protein and NF-κB inhibitor Iκβζ. Blockade of RAGE has therapeutic importance in type 1 DM–mediated DLE within the complex regulation of NF-κB.

Although management of type 1 diabetes mellitus (DM) has improved tremendously, longer life spans have increased long-term complications of DM, including retinopathy, nephropathy, vascular disease, diabetic peripheral neuropathy (1–3), and cognitive decline (4–6). Previously undetected or ignored changes within the brain, described as diabetic leukoencephalopathy (DLE) (4), are associated with cerebral atrophy, cognitive decline, and possibly, white matter abnormalities (4,5,7–9).

There is pathogenic synergy between DLE and Alzheimer's disease, as apolipoprotein processing, impairment in corticosteroid regulation, and disruption of insulin signaling (10–12) occur in both. A pathway implicated in DM complications and Alzheimer's disease is the advanced glycation end product (AGE) pathway (13), with independent toxicity due to magnified oxidative stress and reduced nitric oxide bioavailability. AGEs propagate with hyperglycemia in DM and aging (13), contributing to a corresponding upregulation of the receptor for AGEs (RAGE), a ubiquitously expressed multiligand transmembrane receptor of the immunoglobulin superfamily of cell surface molecules (14).

AGE-RAGE signaling initiates protein kinase pathways such as with proinflammatory gene activation and secondary immune responses (15). Signal transduction cascades activated by RAGE include mitogen-activated protein (MAP) kinases, the Janus kinase–signal transducer and activator of transcription signaling family, cell division control protein 42, RAS-related C3 botulinum substrate 1 and other Ras family members, steroid receptor coactivator-1, SMAD signaling family members, and phosphoinositide 3-kinase (16). A main central transcription factor targeted by RAGE signaling and potentially contributing to DLE pathogenesis is nuclear factor (NF)-κB (17,18), which influences or results from both beneficial and detrimental processes as a responder to stress (19); although chronically elevated NF-κB is considered to be detrimental (20), increased and decreased NF-κB levels may both occur in different disease conditions (21). NF-κB mediates the expression of multiple target genes after nuclear translocation and DNA binding (13,18), with most of these target genes related to immune responses (interleukins [IL]), inflammation (tumor necrosis factor [TNF]-α), apoptosis, and stress responses (22).

Because it is not known whether intensive glycemic control prevents progression of DLE as it does in other DM complications (23), we have targeted RAGE, expanding on previous work demonstrating its role in DLE, where $RAGE^{-/-}$ mice were protected from severity of morphologic, radiologic, and molecular changes in a model of type 1 DM (1). We hypothesized that blockade of the RAGE pathway using soluble RAGE (sRAGE), a competitive decoy, would ameliorate changes of type 1 DM–mediated DLE as with other DM complications (14,24) through prevention of long-term behavioral, structural, and molecular changes.

RESEARCH DESIGN AND METHODS

Animals. We studied 127 male transgenic and wild-type C57BL/6 mice (initial weight, 20–30 g) housed in a strict-pathogen free environment in plastic-covered cages in sawdust, with normal light-dark cycles and free access to mouse chow and water, using protocols approved by the University of Calgary animal care committee using the Canadian Council of Animal Care guidelines. We

From the [1]Department of Clinical Neurosciences and the Hotchkiss Brain Institute, University of Calgary, Calgary, Alberta, Canada; and the [2] Diabetes Research Program, Department of Medicine, Division of Endocrinology, New York University Langone Medical Center, New York, New York.
Corresponding author: Cory C. Toth, corytoth@shaw.ca.
Received 14 March 2012 and accepted 9 July 2012.
DOI: 10.2337/db12-0317
This article contains Supplementary Data online at http://diabetes.diabetesjournals.org/lookup/suppl/doi:10.2337/db12-0317/-/DC1.

studied the fully viable transgenic RAGE$^{-/-}$ mouse (courtesy of A.M.S.), as described previously (25) with a SVEV129_C57BL/6 background (129/B6) (26) back-crossed with a C57BL/6 background more than eight times.

Mice were anesthetized with pentobarbital (60 mg/kg) before all surgical procedures. Additional insulin, fluid delivery, or other treatments were not provided.

Diabetes. At the age of 1 month, 28 RAGE$^{-/-}$ mice and 52 wild-type (WT) mice were injected with intraperitoneal streptozotocin (pH 4.6; Sigma, St. Louis, MO) on three consecutive days with 60, 55, and 50 mg/kg after 8 h of fasting; the remaining 25 RAGE$^{-/-}$ mice and 24 WT mice were similarly injected with carrier (sodium citrate, pH 4.6). Monthly weights, glycemic measurements, definitions of fasting glucose threshold, and exclusion criteria were performed as described previously (5). Studies using harvested tissues occurred after 3 months (32 DM mice, 17 non-DM mice), 5 months (18 DM mice and 12 non-DM mice), and 8 months (29 DM mice, 19 non-DM mice) of DM (>9 months of life).

Daily intraperitoneal sRAGE delivery studies. sRAGE (provided by Dr. Ann Marie Schmidt, Columbia University, New York, NY) was produced in a baculovirus expression system using an Sf9 insect cell line (27). After confirmation of DM, WT and RAGE$^{-/-}$ mice were randomized 1:1 to receive a daily intraperitoneal injection of sRAGE (2 mL/kg or 0.05 mL) or placebo carrier (PBS) for 8 months using blinded delivery. All cohorts contained a minimum of eight mice.

Cognitive behavioral testing. A minimum of eight mice in each cohort underwent weekly cognitive behavioral testing for evaluation of procedural, visuospatial, and recognition memory, as performed and described previously with training regimens (5). In brief, the Holeboard and Radial Arm tests measure foraging tendencies, visuospatial information processing, and long-term memory. The Object Recognition task uses delayed spatial non–matching-to-sample testing evaluating novelty seeking and exploratory behavior. The Morris Water-Maze test examines visuospatial memory. Results were recorded by the same observers for each cohort using one trial each of the Holeboard, Radial Arm, and Object Recognition tests during fasting. After feeding, the Morris Water-Maze test was performed 1 h later (5), followed by warming via a heat lamp. Loss of linear swim or run speed led to discontinuation of cognitive testing (5).

Magnetic resonance imaging (MRI). At 1, 3, 5, and 8 months after DM induction, four or more mice from each cohort underwent MRI scanning as described previously (5). Sequences acquired were T1-weighted images, perfusion-weighted imaging, and diffusion-weighted (DW) images for calculating an apparent diffusion coefficient of water (ADC) map, and T2-weighted images (5) for determining T2 maps over a total of 24 cerebral slices. Newly performed magnetization transfer (MT) images were acquired within four 0.75-mm-thick slices in the midcerebrum using proton density-weighted spin echo images (repetition time, 5,000 ms; echo time, 15 ms) with MT saturation off and on (40 gauss pulses with a power of 4 μT and a frequency offset of 1,500 Hz). For image analysis, MT ratios were calculated as $[(Mo - Ms)/Mo] \times 100\%$, where *Ms* and *Mo* were the signal intensities obtained with and without MT saturation, respectively. Diffusion tensor imaging (DTI), performed only at the 8-month assessment, was used to detect water diffusion within myelinated pathways based on reduction in fractional anisotropy (FA) for type 1 DM mice and correlation with impaired neurocognitive performances (9). Analysis of MRIs was performed using MedINRIA 1.8.0 (INRIA-Asclepios Research Team) for analysis of FA/tractography or with Marevisi (EIC, IBD) for other analyses by an observer with cohort blinding. T1 MRIs permitted volumetric brain measurements via integration of cross-sectional areas for slices multiplied by thickness (0.75 mm) of the MR slices (5).

Harvesting of nervous tissues. Weights of mice and harvested brains and final glycemic values were determined. Euthanasia and harvesting of tissues occurred 6 h after the last intraperitoneal sRAGE or placebo delivery. Whole blood was tested for glycated hemoglobin A_{1c} (HbA_{1c}) and plasma insulin levels were measured (5,28). Harvesting and preservation of brain tissues occurred as described previously (5) for morphologic, immunohistochemical, and biochemical studies, including quantitative (q) real-time RT-PCR, cDNA microarray testing, Western blotting, and electrophoretic mobility shift assays, with storage of brain tissues at −80°C for <1 month.

Brain sectioning and staining. Myelination was visualized by staining paraffin brain sections for Luxol Fast Blue or myelin basic protein (MBP; 1:100, Stemcell Technologies Inc., Vancouver) with a secondary antibody (bovine anti-mouse IgG Cy3, 1:100; Zymed Inc., San Francisco, CA) (5). Neurons were identified with microtubule associated protein (MAP)-2 (1:100, Abcam, Cambridge, MA), and oligodendrocytes were identified with oligodendrocyte-specific protein (OSP) (1:200, Abcam) immunohistochemistry as previously described (28,29). Secondary antibodies were anti-mouse IgG Cy3 (1:200, Zymed Inc.) and anti-rabbit fluorescein isothiocyanate (FITC; 1:200, Zymed Inc), respectively.

Detailed neuronal and oligodendroglial cell counts were performed using standard unbiased stereologic methods for those slides stained with the neural

TABLE 1
Body masses, plasma insulin, glycemia, and mortality rates in DM and non-DM mice

	Time point											
	Month 0		Month 3					Month 8				
	Mass	Blood glucose	Mass	Plasma insulin	Blood glucose	HbA_{1c}	Survival	Mass	Plasma insulin	Blood glucose	HbA_{1c}	Survival
wtplac	25.5 ± 3.8	5.7 ± 2.4	39.5 ± 3.8	270 ± 25	5.9 ± 2.5	4.7± 2.5	18/18 (100)	49.7 ± 3.5	261 ± 21	6.2 ± 2.3	4.9 ± 2.8	9/9 (100)
wtDMplac	25.8 ± 3.5	5.6 ± 2.1	28.5 ± 3.8	<25*	32.5 ± 3.2*	11.2 ± 4.1*	18/20 (90)	31.5 ± 3.6	<25*	32.9 ± 2.6*	13.0 ±3.8*	7/10 (70)
wtDMsRAGE	25.6 ± 3.7	5.6 ± 2.2	28.5 ± 3.8	<25*	32.6 ± 4.0*	10.8 ± 3.9*	18/20 (90)	35.6 ± 3.9	<25*	32.8 ± 2.0*	13.2 ± 3.6*	6/10 (60)
RAGE$^{-/-}$	26.1 ± 3.2	5.7 ± 2.4	40.7 ± 3.8	272 ± 21	5.6 ± 2.3	4.5 ± 2.6	19/19 (100)	52.2 ± 3.8	278 ± 25	5.9 ± 2.4	5.0 ± 3.0	10/10 (100)
RAGE$^{-/-}$DM	26.4 ± 3.4	5.5 ± 2.2	30.2 ± 3.8	<25*	31.9 ± 4.5*	10.7 ± 3.6*	17/20 (85)	33.3 ± 3.8	<25*	32.3 ± 3.8*	12.8 ± 4.0*	7/9 (78)

Survival is presented as *n*/*N* (%) and measures as mean ± SEM. Mass weights are presented in grams, blood glucose values are presented in mmol/L, HbA_{1c} values are presented as percentages, and plasma insulin levels are presented as pmol/L. * $P < 0.05$ using Student *t* test ($\alpha = 0.05$) with wtplac compared with wtDMsRAGE or wtDMplac, and for RAGE$^{-/-}$ mice compared with RAGE$^{-/-}$DM only. Two-tailed testing was used for mass and HbA_{1c} results, whereas one-tailed testing was used for blood glucose and plasma insulin levels.

marker MAP-2 (4,30) and the oligodendroglial marker OSP (28,29) using the optical dissector method (30).

Western immunoblotting. Tissue portions (cortex, hippocampus, thalamus/internal capsule, brainstem) were processed for Western blotting (5). For nuclear proteins, separation of cytosolic and nuclear fractions using centrifugation at 10,000*g* for 15 min at 4°C occurred, with supernatant collected as the cytosolic fraction and the pellet served as nuclear fraction. Resuspension of nuclear fraction pellets was accomplished using 300 μL of homogenization buffer B (1% Triton X-100 in buffer A) with sonication performed for 10 s. The nuclear suspension was further centrifuged at 15,000*g* for 15 min at 4°C, with supernatant then collected as a nuclear lysate fraction. Cytosolic, nuclear, or total fractions were studied using equal amounts (15 μg) of protein separated by SDS-PAGE using 10% polyacrylamide gels under conditions previously described (1).

Blots were probed with antibodies to the AGE *N*-(carboxymethyl)lysine) (anti–*N*-(carboxymethyl)lysine) monoclonal antibody, CosmoBio, Tokyo, Japan, 1:200), RAGE (1:500, courtesy of A.M.S.), NF-κB p65 (1:200, Santa Cruz Biotechnology, Santa Cruz, CA), C-Rel (1:1000, Abgent, Inc., San Diego, CA), inhibitor of NF-κB kinase subunit α (IKKα), phospho-(p)-IKKα, and molecular target of rapamycin (mTOR; 1:1000, Cell Signaling, Danvers, MA), inhibitory subunit NF-κBα/β (IκBα/β), B-cell lymphoma 3-encoded protein (Bcl-3), Toll-like receptor (TLR)2, IL-1β, IL-6, and IL-12 (1:500, Abcam, Cambridge, UK), NF-κB inhibitor (IκB)ζ (1:500, Acris Antibodies, San Diego, CA), and tumor necrosis factor (TNF)-α (1:1000, Millipore, Billerica, MA).

Synaptic presence quantification was performed using anti-synaptophysin (1:1000; Santa Cruz, Santa Cruz, CA polyclonal) and anti-choline acetyltransferase (1:500, Abcam, Cambridge, U.K., polyclonal). Anti–β-actin (1:100, Biogenesis Ltd. Poole, U.K.) was applied to separate blots as a loading control. Secondary anti-rabbit, anti-mouse, or anti-human IgG horseradish peroxidase–linked antibody (Cell Signaling) was applied at 1:5000 in each case as appropriate. Signal detection and analysis was performed as described previously (5).

mRNA quantification. Total RNA was extracted from cortex, hippocampus, and thalamus/internal capsule using Trizol (Invitrogen, Burlington, ON, Canada). Total RNA (1 μg) was processed directly to cDNA synthesis using the Superscript II Reverse Transcriptase system (Invitrogen) (5). Primer sequences (Supplementary Table 1) were used for RT-PCR, performed using SYBR Green

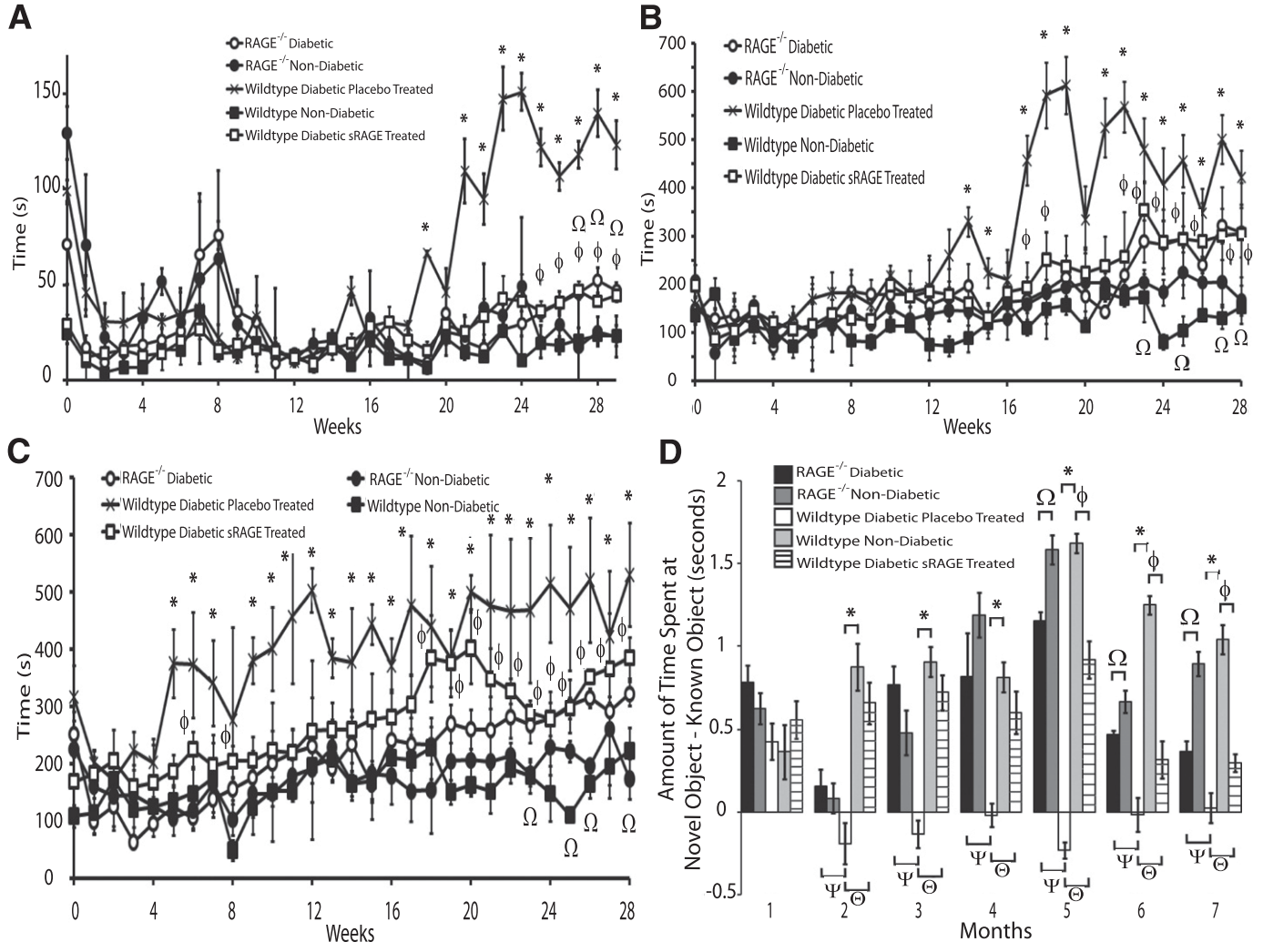

FIG. 1. Cognitive behavioral data. There were no significant baseline differences between any of the mouse cohorts in the first 10 weeks. *A*: In the Morris Water-Maze, latency times to reach the platform began to wane for wtDMplac after 21 weeks, whereas wtDMsRAGE and RAGE$^{-/-}$DM were protected from declining performance until later time points compared with wtplac or RAGE$^{-/-}$. *B*: For the Radial Arm test, similar declines in function were seen for DM mice, with later and less severe deficits witnessed for wtDMsRAGE and RAGE$^{-/-}$DM mice. *C*: In the Holeboard test, earlier decline in function was seen for wtDMplac and for wtDMsRAGE, although later declines in function of RAGE$^{-/-}$DM mice were also noted. *D*: Finally, in the Object Recognition Task, less time was spent at the novel object for wtDMplac beginning from 2 to 7 months, with more severe deficit than seen in wtDMsRAGE or RAGE$^{-/-}$DM mice. For wtDMsRAGE or RAGE$^{-/-}$DM mice, less time spent at the novel object became noted at 5 to 7 months. Repeated-measures ANOVA testing revealed significant differences were identified between cohorts to be compared, indicated, with *wtDMplac vs. wtplac, ΦwtDMsRAGE vs. wtplac, and ΩRAGE$^{-/-}$DM mice vs. RAGE$^{-/-}$. Additional AUC measurements identified significantly improved performances for wtDMsRAGE compared with the wtDMplac and for RAGE$^{-/-}$DM compared with wtDMplac ($P < 0.025$ using Bonferroni corrections) for Morris Water-Maze, Radial Arm, and Holeboard tests. Additional comparisons between RAGE$^{-/-}$DM mice vs. wtDMplacebo and between wtDMplac vs. wtDMsRAGE were performed using repeated-measures ANOVA with appropriate Bonferroni corrections, with significance demonstrated using $\Psi P < 0.025$ and $\Theta P < 0.025$, respectively (n = 8–10 mice in each mouse cohort for each time point).

dye. Data analysis was performed (5) using the housekeeping gene 18S for normalization.

EMSA. EMSA was performed and quantified as described previously (3,5) for cortical and hippocampal tissues. We used 20,000–50,000 cpm of ^{32}P-labeled oligonucleotide (S) corresponding to a NF-κB–binding site (5′-TCGACAGA [[GGG**A**CT**TT**CC]]GAGAGGC-3′), where square brackets indicate the binding region and bold letters indicate nucleotide variability.

cDNA microarrays. Total RNA was isolated from hippocampi/cortex using Trizol reagent (Life Technologies, Inc.). mRNAa were used to generate Cy3-/Cy5-labeled first-strand cDNA via reverse transcription; cDNA products were used for hybridization array slides. Fluorescence-labeled cDNA targets were made using reverse transcription with 1–2 μg of poly(A)+ RNA or 50–100 μg of total RNA incubated in a cocktail containing Cy3 or Cy5-dUTP (Amersham Pharmacia Biotech, Inc., Piscataway, NJ) and SuperScript II RT (Life Technologies, Inc.). Appropriate Cy3 and Cy5 targets were combined along with 2 μL (20 μg) mouse hippocampi/cortex DNA, 1 μL (8–10 μg) poly(A), 2.6 μL 20× SSC, and 0.45 μL 10% SDS in a final volume of 15 μL. After denaturation, labeled targets were added to processed mouse array slides (Signosis, Sunnyvale, CA), then placed in hybridization chambers and incubated overnight (10–16 h) at 65°C. The following day, slides were washed for 1 min in 1× SSC, for 1 min in 0.2× SSC, and for 10 s in 0.05× SSC, and then spun dry. Fluorescence images were captured using a Bio Rad ChemiDoc XRS+ System (Bio Rad, Mississauga, ON, Canada) and analyzed with Photoshop 9.0 (2005, Adobe, San Jose, CA).

Analysis. All data were represented as mean ± SEM. ANOVA testing with multiple comparisons of independently assessed samples and groups were performed in all cases. Cohorts meant to be compared were: WT DM mice receiving placebo (wtDMplac) vs. WT non-DM mice (wtplac); WT DM mice receiving sRAGE (wtDMsRAGE) vs. wtDMplac; and RAGE$^{-/-}$ DM mice (RAGE$^{-/-}$DM) vs. RAGE$^{-/-}$ non-DM mice (RAGE$^{-/-}$). Separate analyses compared RAGE$^{-/-}$DM mice and wtDMplac, as well as wtDMsRAGE and wtplac. For serially collected behavioral data, repeated-measures ANOVA testing was performed, and area under the curve (AUC) statistical testing was performed using trapezoidal methods. Correlational relationships for AUC were tested using multiple linear regression analysis. Survival was analyzed using Kaplan-Meier survival analysis. Bonferroni corrections were applied in all cases for multiple group examinations.

RESULTS

DM. DM was induced within 2 weeks of streptozotocin treatment in greater than 85% of mice and was maintained over the length of the study. DM mice were smaller than non-DM mice throughout life, with unmeasureable plasma insulin levels (Table 1). Hyperglycemia, increases in HbA_{1c}, and survival were similar among wtDMsRAGE, wtDMplac, and RAGE$^{-/-}$DM mice.

Cognitive behavioral data. After 30 weeks of DM, swimming times were significantly prolonged for DM mice and cognitive studies discontinued. DM and non-DM mice had similar learning ability during the initial weeks (Fig. 1). In the Morris Water-Maze task, the performance of wtDMplac was inferior compared with wtplac after 21 weeks of DM (ANOVA $P < 0.05$, $F = 1.88–6.02$). However, RAGE$^{-/-}$DM and wtDMsRAGE performed similarly to comparison cohorts until 25–30 weeks of DM (ANOVA $P < 0.05$, $F = 1.62–2.14$), with late waning function for wtDMsRAGE (ANOVA $P < 0.05$,

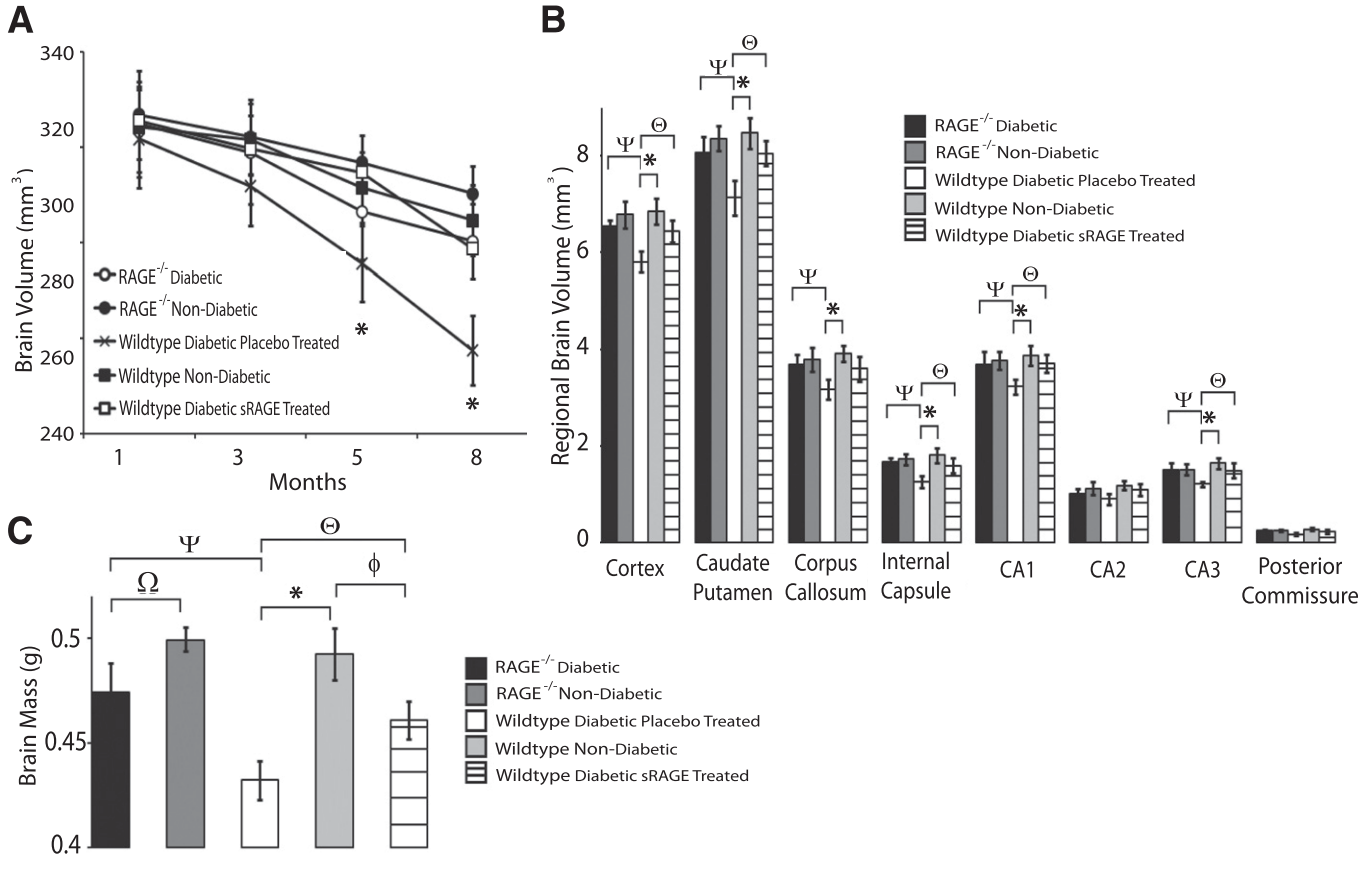

FIG. 2. Brain size measurements. *A*: Volumetric measurements of brain demonstrated diffuse cerebral atrophy after 5 and 8 months only in wtDMplac. *B*: After 8 months, regional atrophy could be detected in the cortex, caudate/putamen, corpus callosum, and in the CA1 portion of hippocampus in wtDMplac. No regional atrophy was present in wtDMsRAGE or in RAGE$^{-/-}$DM mice. Greater regional brain atrophy was found in wtDMplac compared with wtDMsRAGE or RAGE$^{-/-}$DM mice. *C*: Wet brain mass was reduced in wtDMplac after 8 months. Less severe brain mass loss also occurred in wtDMsRAGE and in RAGE$^{-/-}$DM mice. ANOVA testing revealed significant differences between cohorts to be compared, indicated with *wtDMplac vs. wtplac, ΦwtDMsRAGE vs. wtplac, and ΩRAGE$^{-/-}$DM mice vs. RAGE$^{-/-}$. Additional comparisons identified statistically significant differences between other cohorts, identified using ΨP < 0.025 for wtDMplac vs. RAGE$^{-/-}$DM mice and ΘP < 0.025 for wtDMplac vs. wtDMsRAGE (n = 8–10 mice in each mouse cohort for each time point).

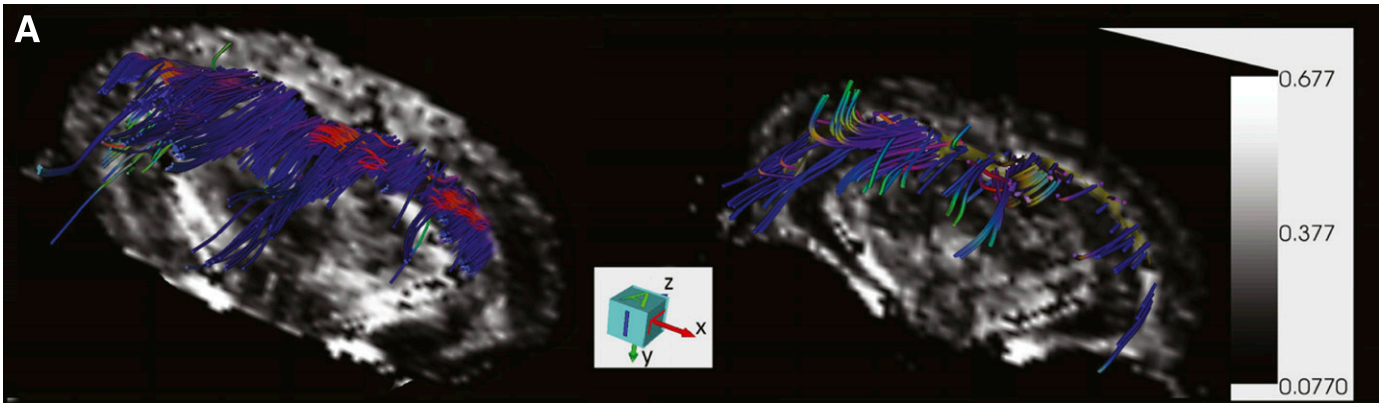
A
0.677
0.377
0.0770
z
x
y

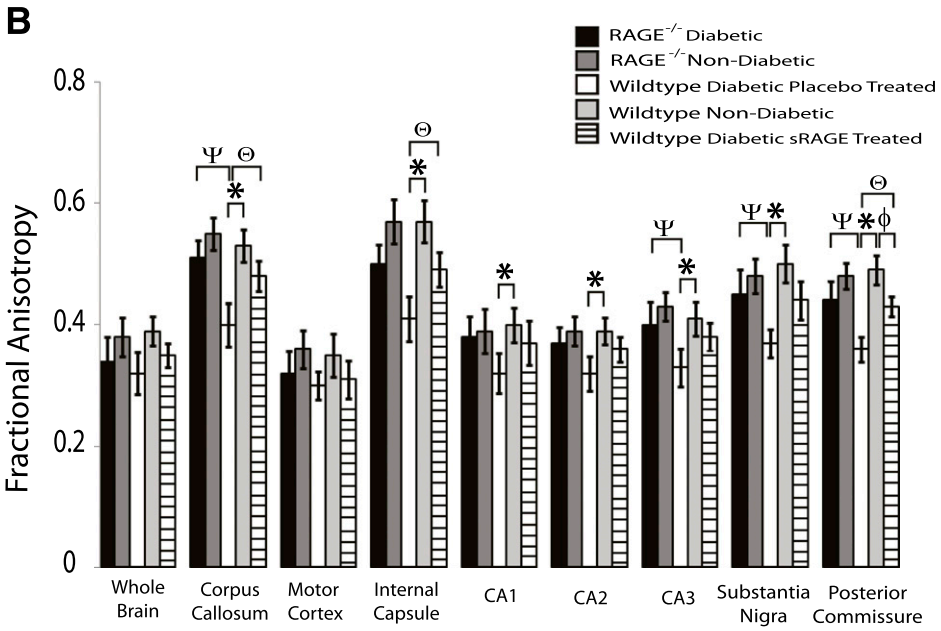
B
RAGE-/- Diabetic
RAGE-/- Non-Diabetic
Wildtype Diabetic Placebo Treated
Wildtype Non-Diabetic
Wildtype Diabetic sRAGE Treated
Fractional Anisotropy
0.8
0.6
0.4
0.2
0
Whole Brain
Corpus Callosum
Motor Cortex
Internal Capsule
CA1
CA2
CA3
Substantia Nigra
Posterior Commissure

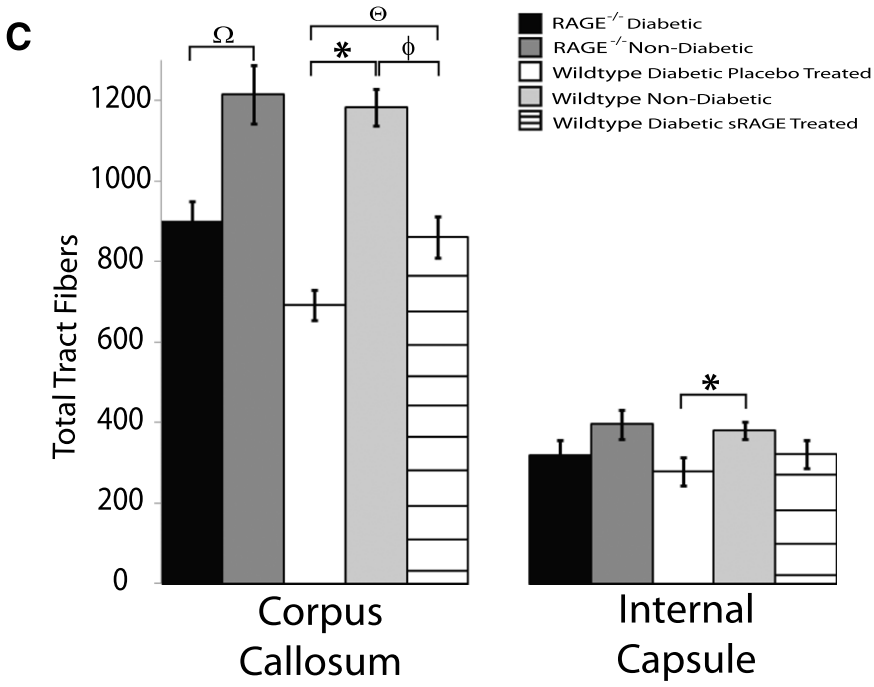
C
RAGE-/- Diabetic
RAGE-/- Non-Diabetic
Wildtype Diabetic Placebo Treated
Wildtype Non-Diabetic
Wildtype Diabetic sRAGE Treated
Total Tract Fibers
1200
1000
800
600
400
200
0
Corpus Callosum
Internal Capsule

F = 1.64–2.35). Overall performance of wtDMsRAGE or RAGE$^{-/-}$DM mice was superior to that of wtDMplac (AUC $P < 0.025$; F = 2.56–4.67).

Similarly, deficits appeared after 14 weeks of DM in the Radial Arm test and after 5 weeks of DM in the Holeboard test for wtDMplac compared with wtplac (ANOVA $P < 0.05$; F = 1.99–8.79). Deficits seen for wtDMsRAGE or RAGE$^{-/-}$DM mice cohorts were milder than those in wtDMplac (AUC $P < 0.025$; F = 2.04–4.14). In the Object Recognition Task, performances waned after 2 months in wtDMplac but only after 5 months in the wtDMsRAGE or RAGE$^{-/-}$DM mice compared with respective cohorts (ANOVA $P < 0.05$; F = 3.05–7.88). However, wtDMsRAGE or RAGE$^{-/-}$DM mice had superior performance after 2 months compared with wtDMplac (ANOVA $P < 0.025$; F = 1.87–7.06).

MRI and brain weight data. Only wtDMplac developed brain atrophy after 5–8 months (ANOVA $P < 0.05$; F = 5.81; Fig. 2). The wtDMsRAGE and RAGE$^{-/-}$DM mice did not develop significant brain atrophy after 8 months (ANOVA P = NS; F = 0.26–0.62). After 8 months, specific regional atrophy was detected in the cortex, caudate/putamen, corpus callosum, internal capsule, and CA1/CA3 hippocampus for wtDMplac (ANOVA $P < 0.05$; F = 0.99–2.35) and was also present in cortex, caudate putamen, and CA1 regions compared with wtDMsRAGE or RAGE$^{-/-}$DM mice (ANOVA $P < 0.025$; F = 1.18–2.06). Loss of brain mass was present after 8 months in wtDMplac (ANOVA $P < 0.05$; F = 3.27); there was less severe brain mass loss in wtDMsRAGE and RAGE$^{-/-}$DM mice (ANOVA $P < 0.025$; F = 1.14–1.22).

MRI T2 values were elevated and MT ratio values were depressed in all brain regions for wtDMplac (ANOVA $P < 0.05$; F = 2.16–8.97; Supplementary Fig. 1). Less severe elevation of T2 map values and loss of MT ratio values was seen for wtDMsRAGE and RAGE$^{-/-}$DM mice for all brain regions (ANOVA $P < 0.025$; F = 2.44–6.72). Similarly, RAGE$^{-/-}$DM mice had less severe T2 map value elevation and MT ratio value depression only within white matter regions (corpus callosum, internal capsule, posterior commissure) and the CA3 hippocampal region (ANOVA $P < 0.025$; F = 0.86–4.51).

After 8 months, DTI identified lowered FA values for wtDMplac in white matter regions (corpus callosum, internal capsule, substantia nigra, posterior commissure) and within the hippocampus (ANOVA $P < 0.05$; F = 0.77–4.04; Fig. 3). In contrast with wtDMplac, FA values were better maintained for wtDMsRAGE and RAGE$^{-/-}$DM mice within white matter regions and CA3 hippocampal region (ANOVA $P < 0.025$; F = 0.82–4.66). The wtDMsRAGE mice had lowered FA values only in the posterior commissure (ANOVA $P < 0.025$; F = 0.46–2.02), whereas RAGE$^{-/-}$DM mice had no compromised FA values (ANOVA P = NS; F = 0.16–0.58). At the internal capsule/corpus callosum, tractography measurements demonstrated lost tracts in wtDMplac (ANOVA $P < 0.05$; F = 3.14–6.79), with less substantial loss in wtDMsRAGE and RAGE$^{-/-}$DM mice (ANOVA $P < 0.025$; F = 1.87–3.05).

Gray and white matter analysis. Neuronal loss occurred in the CA3 region of the hippocampus (but not cortex) after 8 months in wtDMplac (ANOVA $P < 0.05$; F = 2.57; Supplementary Table 2), without any loss of neurons in wtDMsRAGE or RAGE$^{-/-}$DM mice.

Oligodendrocyte density was significantly lower after 3 months in the corpus callosum, internal capsule, and thalamus of wtDMplac (ANOVA $P < 0.05$; F = 2.15; Supplementary Table 3), with further progressive loss after 8 months (ANOVA $P < 0.05$; F = 2.45–3.57). More mild and delayed loss of oligodendrocyte density occurred after 8 months in wtDMsRAGE and RAGE$^{-/-}$DM (ANOVA $P < 0.025$; F = 2.78–6.22).

Myelin and synaptic protein analysis. After 8 months, myelin associated glycoprotein and MBP expression was diminished in wtDMplac (Fig. 4), without loss in RAGE$^{-/-}$DM or wtDMsRAGE mice. Also, synaptic machinery (both synaptophysin and choline acetyltransferase) was quantitatively diminished in wtDMplac, without evidence for synaptic protein loss for RAGE$^{-/-}$DM or in wtDMsRAGE mice, similar to that detected in rat models of DM (28). The above MRI abnormalities, along with changes in myelin proteins, appear related to previously identified loss of myelin with loss of Luxol Fast Blue staining, MBP immunostaining, and dysregulation of myelin-related proteins in the diabetic rodent brain (4,5,29).

RAGE–NF-κB molecular pathways. RAGE protein expression was greatest in wtDMplac after 8 months (Fig. 5), with less upregulation of RAGE protein identified for wtDMsRAGE in cortical and hippocampal regions. Concurrent elevation of C-Rel and NF-κB p65 protein occurred in multiple brain regions with DM, with less significant elevation seen in wtDMsRAGE and in RAGE$^{-/-}$DM mice. Levels of mRNA for *RAGE* and *NF-κB p65* were in keeping with protein results for the cortex and hippocampus (data not shown). EMSA also identified greater NF-κB–DNA interaction in wtDMplac.

cDNA multiarray analysis using hippocampus showed upregulation of most NF-κB–regulated genes occurred after 3 months in wtDMplac, with less upregulation observed in wtDMsRAGE (Supplementary Table 4). However, unexpectedly and notwithstanding upregulation of NF-κB DNA seen with EMSA, almost all NF-κB–regulated genes were downregulated after 8 months (Supplementary Table 5). The only mRNA upregulated in wtDMplac was *TNF-α* (Fig. 6). Owing to this unanticipated finding, we examined

FIG. 3. DTI with FA and tractography measurements performed after 8 months of DM. *A*: Coronal sections of brain through the corpus callosum demonstrate a three-dimensional representation of the planar view of the tracts of the corpus callosum and axes for wtplac (*left*) and wtDMplac (*right*). *B*: FA values were depressed after 8 months of DM for wtDMplac in the corpus callosum, internal capsule, substantia nigra, posterior commissure, and throughout the hippocampus compared with wtplac. wtDMplac had lower FA values then wtDMsRAGE within the corpus callosum, internal capsule, and posterior commissure. In addition, wtDMplac had lower FA values than RAGE$^{-/-}$DM in the corpus callosum, substantia nigra, posterior commissure, and CA3 region of the hippocampus. Relative to wtplac, wtDMsRAGE were only compromised for FA values in the posterior commissure. Meanwhile, RAGE$^{-/-}$ had similar FA values compared with RAGE$^{-/-}$DM. *C*: Tractography calculations performed at the corpus callosum and internal capsule demonstrated a loss of tract fibers for wtDMplac. Similar patterns as with FA measurements were noted for loss of tract fibers and amelioration was seen in wtDMsRAGE and RAGE$^{-/-}$DM mice compared with cohorts to be judged against. ANOVA testing revealed significant differences identified between cohorts to be compared, indicated with *wtDMplac vs. wtplac, ΦwtDMsRAGE vs. wtplac, and ΩRAGE$^{-/-}$DM vs. RAGE$^{-/-}$. Additional comparisons identified statistically significant differences between other cohorts, identified using $\Psi P < 0.025$ for wtDMplac vs. RAGE$^{-/-}$DM and $\Theta P < 0.025$ for wtDMplac vs. wtDMsRAGE (n = 4–6 mice in each mouse cohort). (A high-quality digital representation of this figure is available in the online issue.)

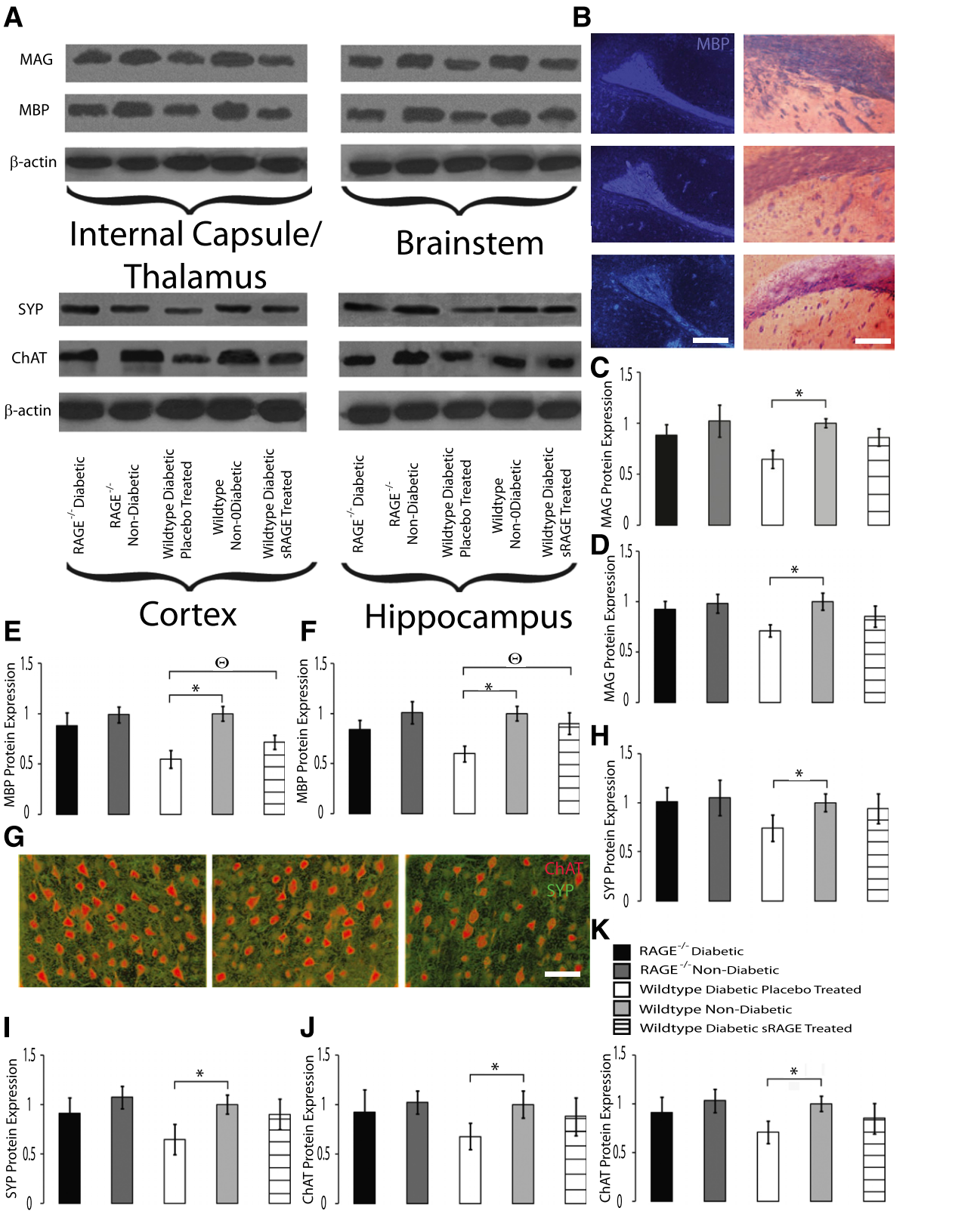

FIG. 4. Myelin and synaptic machinery protein quantifications performed in cortex and hippocampal brain regions after 8 months of DM. *A*: Sample Western blots are demonstrated for myelin-associated glycoprotein (MAG) and myelin basic protein (MBP) from the internal capsule/thalamus and brainstem regions and for synaptophysin (SYP) and choline acetyltransferase (ChAT) from the cortex and hippocampus. *B*: Examples of immunohistochemistry for myelin basic protein (*left*) and Luxol Fast Blue (*right*) histochemistry are demonstrated for wtplac (*top*), wtDMsRAGE (*middle*), and wtDMplac (*bottom*) (bar = 0.5 mm). Quantitative expression for MAG in the internal capsule/thalamus (*C*) and brainstem (*D*) showed downregulation of this myelin protein in wtDMplac and absence of loss in RAGE$^{-/-}$DM and in wtDMsRAGE. Similarly, MBP expression was downregulated in the internal capsule/thalamus (*E*) and brainstem (*F*) for wtDMplac compared with wtplac, without significant loss of MBP in RAGE$^{-/-}$DM or in wtDMsRAGE. *G*: Immunohistochemical examples of SYP and ChAT are codemonstrated for wtplac (*left*), wtDMsRAGE (*middle*), and wtDMplac (*right*) (bar = 50 μm). Synaptic protein SYP expression was diminished for wtDMplac in the cortex (*H*) and hippocampus (*I*)

further NF-κB–associated regulatory mechanisms. Our assessments of cytosolic (IκBα and IκBβ) and nuclear (IκBβ) protein expression showed downregulation of all IκB proteins in wtDMplac. Protein levels for each of p-IKKα and IKKα (cytosolic and nuclear) were all upregulated in wtDMplac but not in RAGE$^{-/-}$DM or in wtDMsRAGE. Levels of mRNA for total IKKα and TNF-α were in keeping with protein results and cDNA multiarray results (data not shown).

Inflammatory and stress-mediated molecular pathways. After 8 months of DM, p-mTOR, TLR2, and TNF-α were upregulated in the cortex/hippocampus for wtDMplac but the change more mild or stable for RAGE$^{-/-}$DM and wtDMsRAGE mice. IL1-β, IL-6, and IL-12 (Fig. 7) demonstrated transient upregulation after 1 to 5 months before a decline in levels back to baseline or even relative deficiency at 8 months. For RAGE$^{-/-}$DM mice and wtDMsRAGE, the transient increase in ILs was milder and without evidence of deficiency after 8 months.

Potential interruptions in the RAGE–NF-κB molecular pathways. Protein levels for IκBζ and Bcl-3 in the nucleus increased steadily within the hippocampi of wtDMplac, but with less prominence in wtDMsRAGE and not at all for RAGE$^{-/-}$DM mice.

DISCUSSION

Our results support previous work showing that experimental type 1 DM is a cause of cognitive decline, brain atrophy, and white matter abnormalities (5,28,31,32). These effects transpose through adolescent and adult years (6). Previous work has identified absence of cerebral microvascular luminal stenosis in type 1 DM mice along with an absence of hypoperfusion on perfusion-weighted MRI studies (5,28), possibly related to relative hypotension in type 1 DM mice. This distinguishes our results from human studies of leukoencephalopathy, where hypertension is a contributing factor and whose presence in rat models contributes to vascular stenoses and cerebral hypoperfusion (28). Although we showed that suppression of RAGE signaling in wtDMsRAGE or RAGE$^{-/-}$DM partially or completely alleviated aspects of DLE, our hypothesis of RAGE hyperactivation leading to chronic unhindered NF-κB–regulated gene activation may not be correct. Although NF-κB mRNA, protein, and their interaction with DNA were undeniably upregulated in a RAGE-dependent manner, NF-κB–regulated genes other than TNF-α were all downregulated unexpectedly after 8 months of type 1 DM. We postulate that this disconnection may be due to the increasing presence of the inducible nuclear proteins IκBζ and Bcl-3 further transactivating or modulating NF-κB–regulated transcription. Together, these results point to a complex and temporally regulated RAGE-mediated pathway playing a role in DLE.

Sustained hyperglycemia is a driving factor for AGE accumulation in DM, with AGE-RAGE ligation instigating subsequent RAGE upregulation (13). Although AGEs contribute to cellular toxicity independent of RAGE ligation (14), AGE-RAGE ligation stimulates a number of signal transduction pathways (15). RAGE pathways related to NF-κB activation, such as with TLR2 (33) and mTOR (34), could be contributing to the late stages of DLE. Other than its specific decameric DNA sequence binding, NF-κB regulates additional cellular activities such as with proliferation, differentiation, and survival. The main NF-κB proteins, RelA (p65), RelB, c-Rel, NF-κB1, and NF-κB2 also play heterogenous roles (35). In the brain, NF-κB is highly upregulated in neurons with greater neuronal activity, influencing synaptic function and neuronal plasticity. NF-κB is also expressed by glia, including oligodendrocytes (36). Outside of NF-κB, RAGE activates mitogen-activated protein (MAP) kinases, Janus kinase–signal transducer and activator of transcription, cell division control protein 42, Ras-related C3 botulinum toxin substrate 1, and other Ras components, steroid receptor coactivator-1, SMADs, and phosphoinositide 3-kinase (35). We postulate that RAGE incites early and late upregulation of NF-κB promotion; although other promoters of NF-κB–regulated transcription, such as IL-6 and IL-12 (37,38), were upregulated early, both showed subsequent downregulation or return to baseline after 8 months of DM. The role of NF-κB role in DLE may be minimized in the later stages of DLE due to potential interference from the increasing presence of nuclear Bcl-3 and IκBζ, and possibly, IKKα.

One example of a RAGE-independent important stimulus for classical NF-κB pathway activation is TNF-α. Although TNF-α was upregulated at the final end point, other NF-κB–mediated genes, such as with IL-1β (39), were not. TNF-α associates with NFKB receptor 1 (tumor necrosis factor receptor 1), leading to cell membrane recruitment of different protein adaptors, as well as stimulating IKKα/IKKβ complex formation in the TNFR1 signaling complex (35). These processes lead to IKKβ activation and phosphorylation of IκB (IκBα or IκBβ) and subsequent proteasomal degradation (35), permitting nuclear entrance/export of particular NF-κB complexes (40). In DM, TNF-α plays an important role in promotion of endothelial dysfunction, inhibition of insulin signaling pathway–associated kinases, and in NF-κB pathway promotion (35). Although these functions can be RAGE-independent, RAGE signaling also regulates TNF-α expression (35). Our results identified upregulation of TNF-α expression in the cortex/hippocampus in wtDMplac, whereas RAGE blockade attenuated this response. In addition, IKKα and IKKβ were upregulated with DM but attenuated with RAGE blockade or absence. Activated IKKβ phosphorylates IκB, inducing ubiquitination and proteasomal degradation (35). Indeed, downregulation of all IκB proteins occurred with DM, which did not lead to anticipated unchecked NF-κB–regulated gene transcription (35). IKKβ recruitment to the promoter of specific NF-κB target genes may possibly occur based on TNF-α signaling (35), affecting eventual transcription and antagonizing normal upregulation of NF-κB–mediated gene transcription. Further potential modulators of NF-κB–mediated gene transcription include Bcl-3 and IκBζ. Bcl-3 inhibits NF-κB–mediated transcription through complexing

compared with wtplac. In contrast, there was no loss of SYP protein in RAGE$^{-/-}$DM or in wtDMsRAGE. Another synaptic protein, ChAT, showed a reduction in expression in the cortex (*J*) and hippocampus (*K*) in wtDMplac compared with wtplac; there was also no detectable loss of ChAT in RAGE$^{-/-}$DM mice or in wtDMsRAGE. ANOVA testing revealed significant differences identified between cohorts to be compared, indicated with *wtDMplac vs. wtplac. Additional comparisons identified statistically significant differences between other cohorts, identified using $\Theta P < 0.025$ for wtDMplac vs. wtDMsRAGE (n = 4–8 Western blots in each mouse cohort). (A high-quality digital representation of this figure is available in the online issue.)

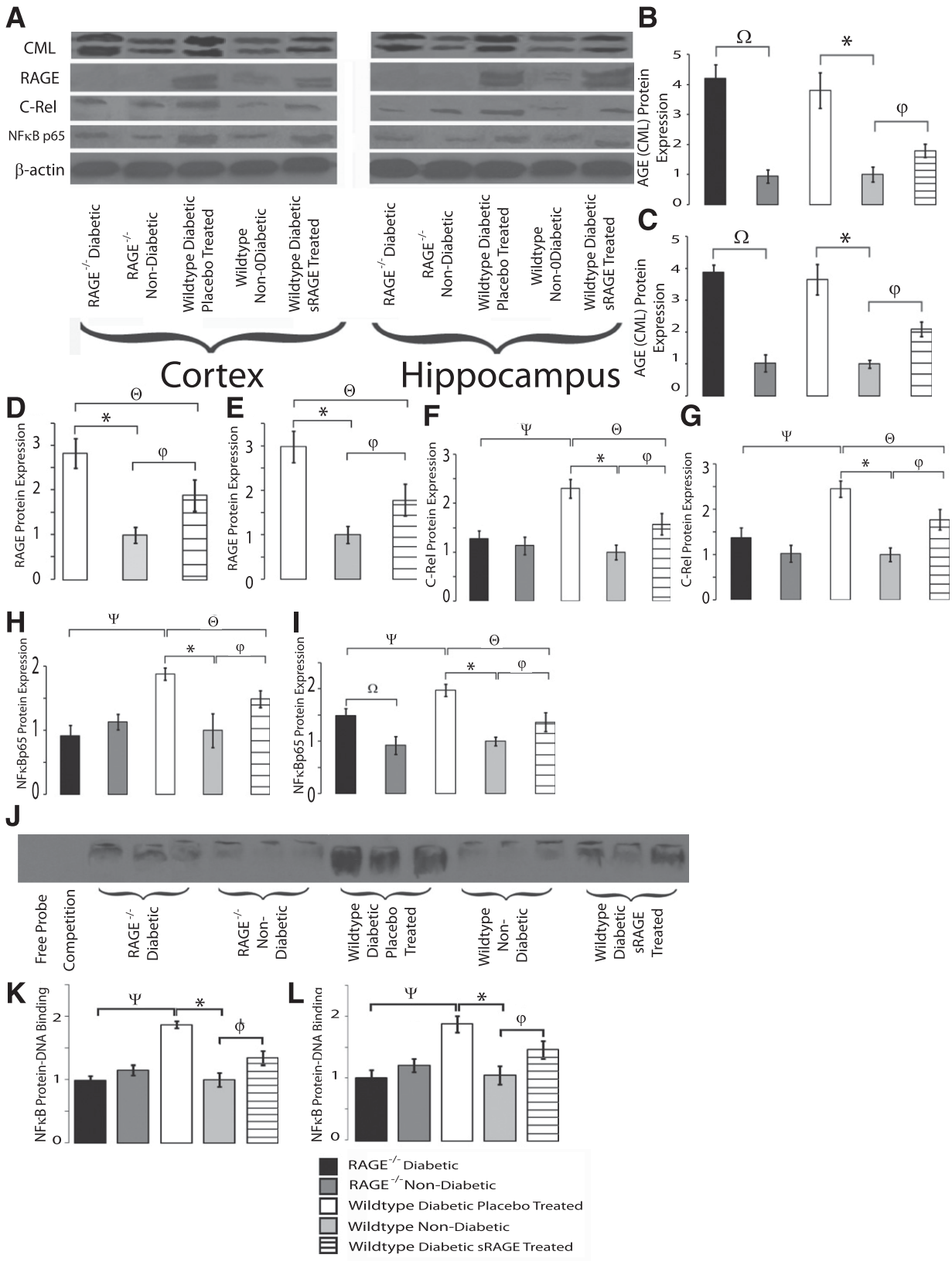

FIG. 5. RAGE and NF-κB–related protein, protein-DNA interaction, and mRNA quantifications for the cortex and hippocampal regions of the brain after 8 months of DM. *A*: Western blots from the cortical and hippocampal regions are demonstrated for the proteins *N*-(carboxymethyl)lysine) (CML; an AGE), RAGE, NF-κB p65, C-Rel, and the housekeeping protein β-actin. Quantitative AGE expression for CML, perhaps the most stable form of AGE, was elevated in the cortex (*B*) and hippocampus (*C*) in mice with type 1 DM, whereas sRAGE provision led to less upregulation. In the cortex (*D*) and hippocampus (*E*), quantitative RAGE expression was greatest in wtDMplac, with less upregulation of RAGE protein noted for wtDMsRAGE. C-Rel protein was also elevated in wtDMplac for the cortex (*F*) and hippocampus (*G*), with less upregulation of C-Rel in RAGE$^{-/-}$DM and wtDMsRAGE. As well, NF-κB p65 protein was similarly elevated in wtDMplac for the cortex (*H*) and hippocampus (*I*), with lesser upregulation noted in RAGE$^{-/-}$DM and wtDMsRAGE mice for the cortical and hippocampal regions. *J*: Examples of EMSAs are shown for hippocampal samples

with NF-κB p50 subunits (41), but activates transcription through complexes with the NF-κB p52 subunit (42), leading to facilitated transcription of TNF-α (43), but not IL-6 or IL-10 (43,44). IκBζ is minimally present during resting stages but is quickly induced with stimulation, followed by nuclear translocation and association with NF-κB p50/p65 (45), resulting in induction and inhibition of NF-κB–regulated transcriptional activity. Interestingly, the transcription of IκBζ is rapidly induced by TLR ligands (46), and IκBζ is critical for TLR-mediated induction of numerous inflammatory genes activated in TLR/IL-1R signaling pathways (37). Also, Bcl-3 forms a ternary complex with DNA and p50 homodimers, leading to repression of gene expression (47). Together, the heightened presence of IKKβ, Bcl-3, and IκBζ increase the complexity in the regulation of NF-κB–dependent gene transcription in DLE.

Limitations of our results must be recognized. All results were obtained within the limits of a murine model, which does not necessarily infer that the same processes occur in the human diabetic brain. The onset of cognitive impairments varied for the behavioral tests performed, anxiety might have contributed to early poor performances during Holeboard testing, and earlier dysfunctional executive function at the prefrontal brain regions might explain earlier abnormalities for Object Recognition tasks.

We attempted to control for concurrent diabetic peripheral neuropathy, but retinopathy, cachexia, ketosis, and other unmeasured metabolic derangements (including measured but untreated severe hyperglycemia) might have confounded our findings. We did not provide insulin therapy to the mice in this study, but our previous results indicate that subcutaneous insulin provides incomplete glycemic improvement without significant improvement in cognition unless insulin is delivered intranasally (5).

The importance of sRAGE delivery or RAGE knockout status on protection from cognitive deficits may be due to a combination of sparing white matter tract abnormalities, synaptic loss, and neuronal dysfunction; we could not separate the individual effects of these on cognition. Functional abnormalities preceded detection of pathologic features, and we speculate that this is due to myelin, neuronal, and synaptic dysfunction occurring earlier than pathologically evident changes. We assume that the distribution of sRAGE is systemic, but the nervous system distribution of sRAGE was not verified. NF-κB upregulation may not relate solely to RAGE ligation and signaling, and certainly could be related to TNF-α, mTOR, and TLR2 upregulation. We cannot rule out the presence of other potential repressors for NF-κB–mediated gene transcription outside of Bcl-3, IκBζ, and IKKα. Also, changes in NF-κB–related proteins may result from neuronal or oligodendroglial loss. Analysis of immunohistochemical sections was not performed, although prior testing identified similar downregulations in synaptic and myelin proteins (4,5). Nevertheless, our results indicate strong evidence for hyperglycemia-mediated upregulation of RAGE in DLE, leading to cognitive decline, brain atrophy, and white matter abnormalities with oligodendroglial and synaptic loss.

Our results indicate that RAGE is an important factor in type 1 DM–mediated DLE. Although not necessarily analogous to the treated type 1 DM patient, our results indicate that AGE-RAGE is a modifiable pathway with potential intervention using sRAGE, the benefits of which extend beyond only DLE. Although intensive glycemic control is important in the progression of diabetic peripheral neuropathy (48), this is unclear in DLE (49). As patients with type 1 live longer, greater effects of DLE will be witnessed. Thus, without intervention, we can anticipate that the role of DM in dementia will magnify both clinically and economically.

ACKNOWLEDGMENTS

This study was supported by an operating grant from the Alberta Heritage Foundation for Medical Research. C.T. is a Clinical Investigator of the Alberta Heritage Foundation for Medical Research. A.M.S is the Iven Young Professor of Endocrinology at New York University.

No potential conflicts of interest relevant to this article were reported.

N.R. performed most of the research studies, portions of the data analysis, and edited the manuscript. K.X., J.L., J.A.M., M.A.H., G.S.S., D.H., P.L., A.A., and K.T. contributed to portions of the studies and edited the manuscript. L.L.R. assisted with provision of the knockout mice and sRAGE for the study. A.M.S. contributed knowledge regarding biochemical pathways, contributed the knockout mice and sRAGE for the study, and edited the manuscript. C.C.T. conceived of the idea, wrote the manuscript, performed some of the research studies listed, researched the data, and performed most of the data analyses. C.C.T. is the guarantor of this work, and, as such, had full access to all the data in the study and takes responsibility for the integrity of data and the accuracy of data analysis.

REFERENCES

1. Toth C, Rong LL, Yang C, et al. Receptor for advanced glycation end products (RAGEs) and experimental diabetic neuropathy. Diabetes 2008; 57:1002–1017
2. Zochodne DW. Diabetes mellitus and the peripheral nervous system: manifestations and mechanisms. Muscle Nerve 2007;36:144–166
3. Francis G, Martinez J, Liu W, et al. Intranasal insulin ameliorates experimental diabetic neuropathy. Diabetes 2009;58:934–945
4. Toth C, Schmidt AM, Tuor UI, et al. Diabetes, leukoencephalopathy and rage. Neurobiol Dis 2006;23:445–461
5. Francis GJ, Martinez JA, Liu WQ, et al. Intranasal insulin prevents cognitive decline, cerebral atrophy and white matter changes in murine type I diabetic encephalopathy. Brain 2008;131:3311–3334
6. Biessels GJ, Deary IJ, Ryan CM. Cognition and diabetes: a lifespan perspective. Lancet Neurol 2008;7:184–190
7. Biessels GJ, De Leeuw FE, Lindeboom J, Barkhof F, Scheltens P. Increased cortical atrophy in patients with Alzheimer's disease and type 2 diabetes mellitus. J Neurol Neurosurg Psychiatry 2006;77:304–307
8. Manschot SM, Brands AM, van der Grond J, et al.; Utrecht Diabetic Encephalopathy Study Group. Brain magnetic resonance imaging correlates of impaired cognition in patients with type 2 diabetes. Diabetes 2006;55: 1106–1113
9. Kodl CT, Franc DT, Rao JP, et al. Diffusion tensor imaging identifies deficits in white matter microstructure in subjects with type 1 diabetes that

demonstrating levels of NF-κB–DNA interaction. NFκB–DNA binding levels were upregulated in wtDMplac for the cortex (*K*) and hippocampus (*L*); again, less upregulation was identified for RAGE$^{-/-}$DM and wtDMsRAGE for both brain regions. NF-κB p65 mRNA was also upregulated in wtDMplac or wtDMsRAGE for the cortex (*M*) or hippocampus (*N*), although upregulation was greater in wtDMplac mice. There was no upregulation of NF-κB p65 mRNA in RAGE$^{-/-}$DM compared with RAGE$^{-/-}$. ANOVA testing revealed significant differences among cohorts to be compared, indicated with *wtDMplacebo vs. wtplac and ΦwtDMsRAGE vs. wtplac. Additional comparisons identified statistically significant differences between other cohorts, identified using Ψ*P* < 0.025 for wtDMplac vs. RAGE$^{-/-}$DM and Θ*P* < 0.025 for wtDMplac vs. wtDMsRAGE (*n* = 4–8 Western blots, EMSA assessments, or mRNA assessments in each mouse cohort).

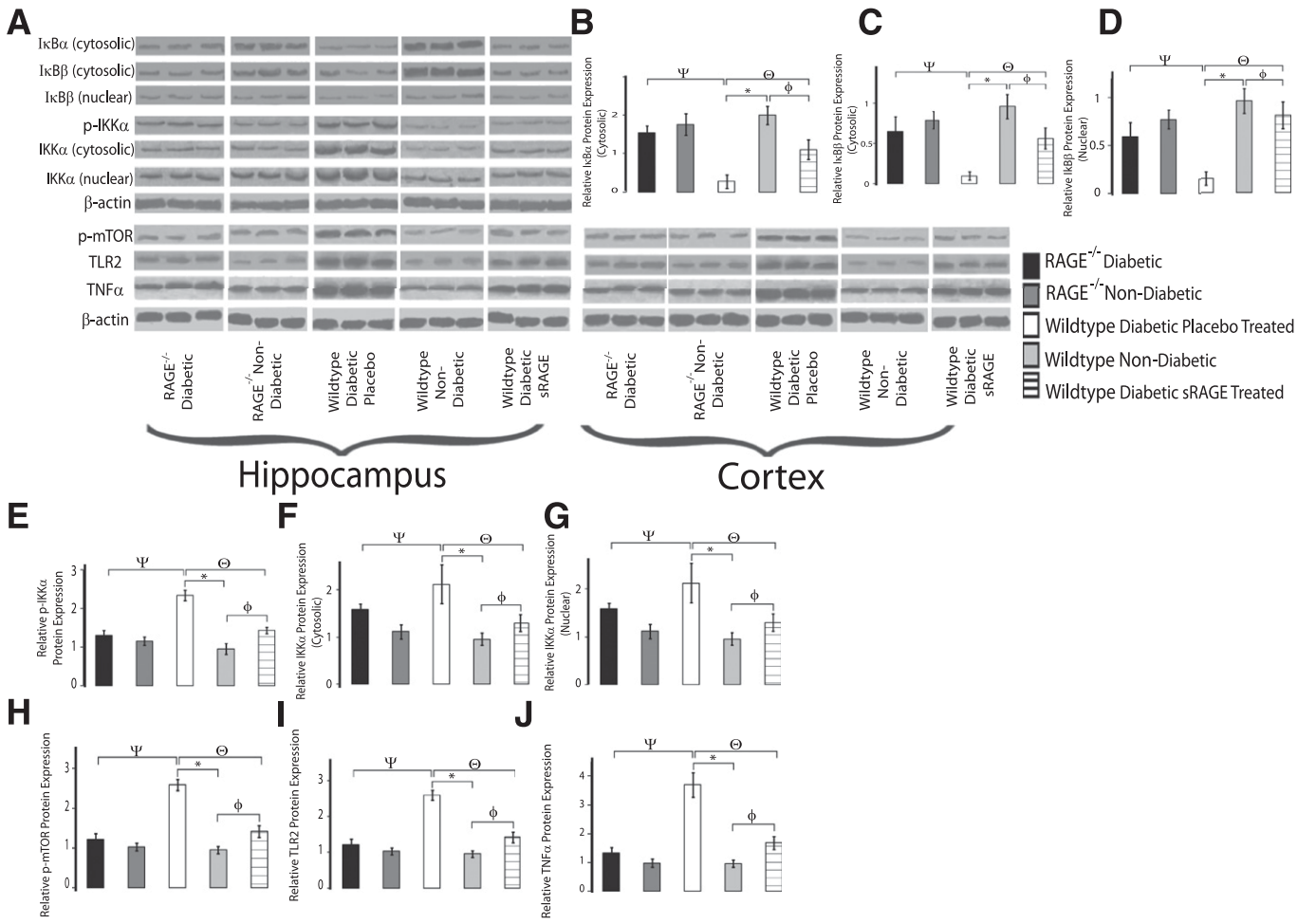

FIG. 6. ***A*: Western blot samples from the hippocampus and cortex are shown for NF-κB proteins and for proteins important in regulation of NF-κB after 8 months of DM. Quantitative graphs are for samples obtained from hippocampus. We also used quantitative RT-PCR to examine important mRNA levels. Cytosolic IκBα (*B*), cytosolic IκBβ (*C*), and nuclear IκBβ protein (*D*) were severely downregulated in wtDMplac compared with wtplac, wtDMsRAGE, and RAGE$^{-/-}$DM. *E*: In contrast, p-IKKα protein was upregulated in wtDMplac compared with wtplac, wtDMsRAGE, and RAGE$^{-/-}$DM. Similarly, cytosolic (*F*) and nuclear (*G*) IKKα protein was upregulated for wtDMplac compared with other cohorts. For wtDMplac, there was also upregulation of proteins for p-mTOR) (*H*), TLR2 (*I*), and TNF-α (*J*); β-actin was used as a housekeeping protein. ANOVA testing revealed significant differences identified among cohorts to be compared, indicated with *wtDMplac vs. wtplac and ΦwtDMsRAGE vs. wtplac. Additional comparisons identified statistically significant differences among other cohorts, as shown by Ψ*P* < 0.025 for wtDMplac vs. RAGE$^{-/-}$DM and Θ*P* < 0.025 for wtDMplac vs. wtDMsRAGE (*n* = 4–8 Western blots or real-time PCR were performed in each mouse cohort).**

correlate with reduced neurocognitive function. Diabetes 2008;57:3083–3089
10. Reddy VP, Zhu X, Perry G, Smith MA. Oxidative stress in diabetes and Alzheimer's disease. J Alzheimers Dis 2009;16:763–774
11. Zhao WQ, Townsend M. Insulin resistance and amyloidogenesis as common molecular foundation for type 2 diabetes and Alzheimer's disease. Biochim Biophys Acta 2009;1792:482–496
12. Stranahan AM, Arumugam TV, Cutler RG, Lee K, Egan JM, Mattson MP. Diabetes impairs hippocampal function through glucocorticoid-mediated effects on new and mature neurons. Nat Neurosci 2008;11:309–317
13. Brownlee M. The pathobiology of diabetic complications: a unifying mechanism. Diabetes 2005;54:1615–1625
14. Wautier JL, Guillausseau PJ. Advanced glycation end products, their receptors and diabetic angiopathy. Diabetes Metab 2001;27:535–542
15. Yan SF, Ramasamy R, Schmidt AM. Receptor for AGE (RAGE) and its ligands – cast into leading roles in diabetes and the inflammatory response. J Mol Med (Berl) 2009;87:235–247
16. Reddy MA, Li SL, Sahar S, et al. Key role of Src kinase in S100B-induced activation of the receptor for advanced glycation end products in vascular smooth muscle cells. J Biol Chem 2006;281:13685–13693
17. Zeng S, Feirt N, Goldstein M, et al. Blockade of receptor for advanced glycation end product (RAGE) attenuates ischemia and reperfusion injury to the liver in mice. Hepatology 2004;39:422–432
18. Bierhaus A, Schiekofer S, Schwaninger M, et al. Diabetes-associated sustained activation of the transcription factor nuclear factor-kappaB. Diabetes 2001;50:2792–2808
19. Perkins ND. The Rel/NF-kappa B family: friend and foe. Trends Biochem Sci 2000;25:434–440
20. Baeuerle PA, Baltimore D. NF-kappa B: ten years after. Cell 1996;87:13–20
21. Yamamoto Y, Gaynor RB. Role of the NF-kappaB pathway in the pathogenesis of human disease states. Curr Mol Med 2001;1:287–296
22. Bianchi R, Giambanco I, Donato R. S100B/RAGE-dependent activation of microglia via NF-kappaB and AP-1: co-regulation of COX-2 expression by S100B, IL-1beta and TNF-alpha. Neurobiol Aging 2010;31:665–677
23. The Diabetes Control and Complications Trial Research Group. The effect of intensive diabetes therapy on the development and progression of neuropathy. Ann Intern Med 1995;122:561–568
24. Goova MT, Li J, Kislinger T, et al. Blockade of receptor for advanced glycation end-products restores effective wound healing in diabetic mice. Am J Pathol 2001;159:513–525
25. Schwenk F, Baron U, Rajewsky K. A cre-transgenic mouse strain for the ubiquitous deletion of loxP-flanked gene segments including deletion in germ cells. Nucleic Acids Res 1995;23:5080–5081
26. Wendt T, Tanji N, Guo J, et al. Glucose, glycation, and RAGE: implications for amplification of cellular dysfunction in diabetic nephropathy. J Am Soc Nephrol 2003;14:1383–1395

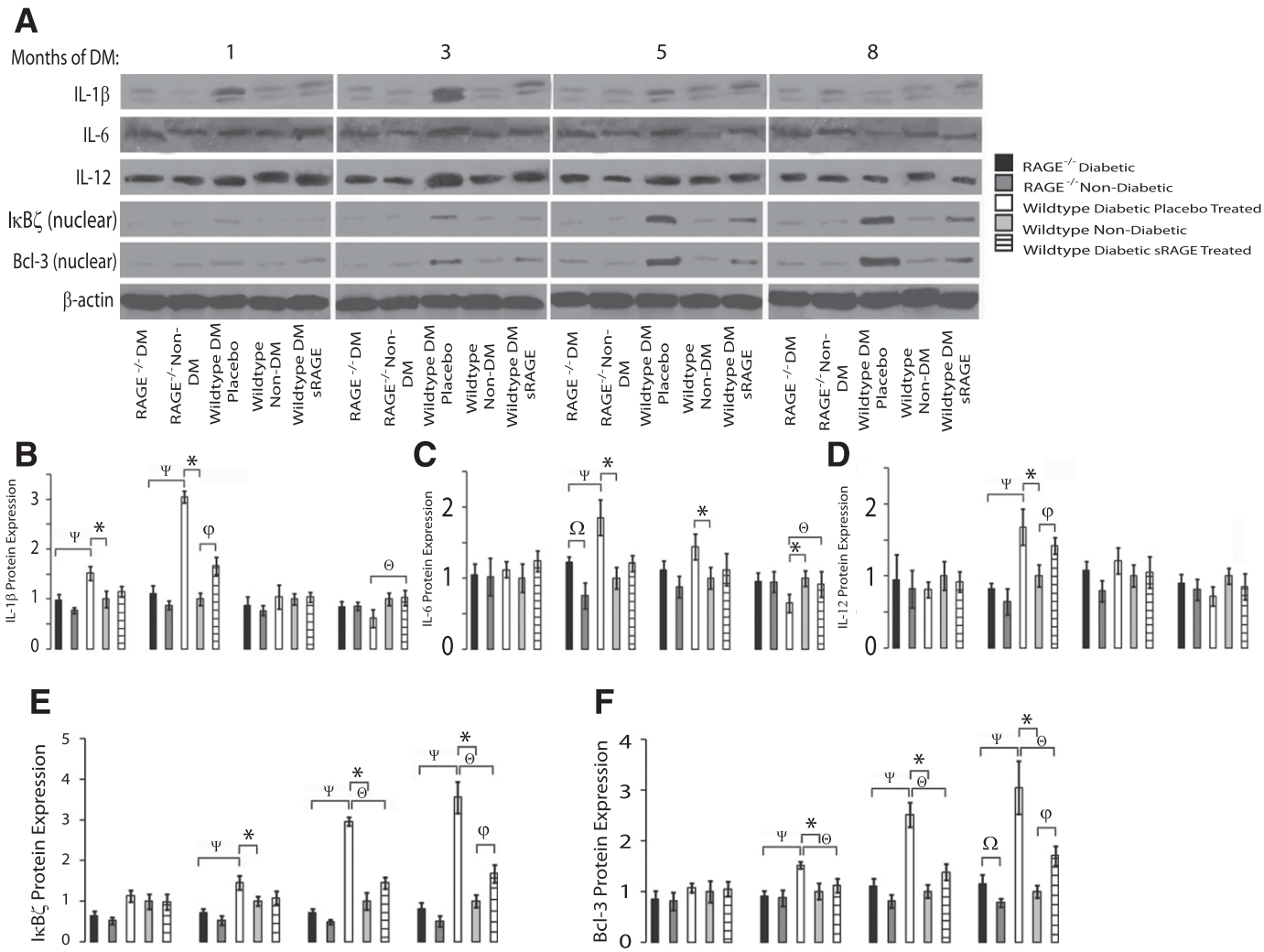

FIG. 7. *A*: Western blots from hippocampi are shown for IL inflammatory proteins and for proteins with ability to disrupt NF-κB–regulated transcription, with β-actin used as the housekeeping protein. Blots were obtained for mice after each of 1, 3, 5, and 8 months of DM, as indicated. For each of IL-1β (*B*), IL-6 (*C*), and IL-12 (*D*), the presence of DM led to transient elevations in each IL after 1 to 5 months of DM, with a subsequent return to baseline or deficiency after 8 months of DM. Increases in IL-1β, IL-6, and IL-12 were modest or nonsignificant, with wtDMsRAGE demonstrating no deficiency in IL proteins after 8 months. Nuclear levels of the proteins IκBζ and Bcl-3 were also measured at each time point. *E*: After 1 month of DM, levels of nuclear IκBζ were unchanged; however, progressive increases in nuclear IκBζ occurred after 3 months until 8 months of DM in wtDMplac compared with wtplac, wtDMsRAGE, and RAGE$^{-/-}$DM. There were more modest increases in nuclear IκBζ protein levels only after 8 months of DM. Similarly, Bcl-3 was elevated in wtDMplac compared with wtplac, with subsequent progressive increases seen after 3 months of DM until 8 months of DM. As with IκBζ, Bcl-3 nuclear protein levels had more moderate rises in wtDMsRAGE and in RAGE$^{-/-}$DM. ANOVA testing revealed significant differences identified among cohorts to be compared, indicated with *wtDMplac vs. wtplac and ΦwtDMsRAGE vs. wtplac. Additional comparisons identified statistically significant differences between other cohorts, identified using ΨP < 0.025 for wtDMplac vs. RAGE$^{-/-}$DM and ΘP < 0.025 for wtDMplac vs. wtDMsRAGE (n = 4–8 Western blots performed in each mouse cohort).

27. Park L, Raman KG, Lee KJ, et al. Suppression of accelerated diabetic atherosclerosis by the soluble receptor for advanced glycation endproducts. Nat Med 1998;4:1025–1031
28. Devisser A, Yang C, Herring A, et al. Differential impact of diabetes and hypertension in the brain: adverse effects in grey matter. Neurobiol Dis 2011;44:161–173
29. Yang C, DeVisser A, Martinez JA, et al. Differential impact of diabetes and hypertension in the brain: adverse effects in white matter. Neurobiol Dis 2011;42:446–458
30. Gundersen HJ, Bendtsen TF, Korbo L, et al. Some new, simple and efficient stereological methods and their use in pathological research and diagnosis. APMIS 1988;96:379–394
31. Brands AM, Biessels GJ, Kappelle LJ, et al.; Utrecht Diabetic Encephalopathy Study Group. Cognitive functioning and brain MRI in patients with type 1 and type 2 diabetes mellitus: a comparative study. Dement Geriatr Cogn Disord 2007;23:343–350
32. Dahlquist G, Källén B; Swedish Childhood Diabetes Study Group. School performance in children with type 1 diabetes–a population-based register study. Diabetologia 2007;50:957–964
33. Wajant H, Henkler F, Scheurich P. The TNF-receptor-associated factor family: scaffold molecules for cytokine receptors, kinases and their regulators. Cell Signal 2001;13:389–400
34. Ghosh S, Tergaonkar V, Rothlin CV, et al. Essential role of tuberous sclerosis genes TSC1 and TSC2 in NF-kappaB activation and cell survival. Cancer Cell 2006;10:215–226
35. Oeckinghaus A, Hayden MS, Ghosh S. Crosstalk in NF-κB signaling pathways. Nat Immunol 2011;12:695–708
36. Małek R, Borowicz KK, Jargiełło M, Czuczwar SJ. Role of nuclear factor kappaB in the central nervous system. Pharmacol Rep 2007;59:25–33
37. Yamamoto M, Yamazaki S, Uematsu S, et al. Regulation of Toll/IL-1-receptor-mediated gene expression by the inducible nuclear protein IkappaBzeta. Nature 2004;430:218–222
38. Grohmann U, Belladonna ML, Bianchi R, et al. IL-12 acts directly on DC to promote nuclear localization of NF-kappaB and primes DC for IL-12 production. Immunity 1998;9:315–323
39. Osborn L, Kunkel S, Nabel GJ. Tumor necrosis factor alpha and interleukin 1 stimulate the human immunodeficiency virus enhancer by activation of the nuclear factor kappa B. Proc Natl Acad Sci U S A 1989;86:2336–2340

40. Hoffmann A, Levchenko A, Scott ML, Baltimore D. The IkappaB-NF-kappaB signaling module: temporal control and selective gene activation. Science 2002;298:1241–1245
41. Watanabe N, Iwamura T, Shinoda T, Fujita T. Regulation of NFKB1 proteins by the candidate oncoprotein BCL-3: generation of NF-kappaB homodimers from the cytoplasmic pool of p50-p105 and nuclear translocation. EMBO J 1997;16:3609–3620
42. Bours V, Franzoso G, Azarenko V, et al. The oncoprotein Bcl-3 directly transactivates through kappa B motifs via association with DNA-binding p50B homodimers. Cell 1993;72:729–739
43. Kuwata H, Watanabe Y, Miyoshi H, et al. IL-10-inducible Bcl-3 negatively regulates LPS-induced TNF-alpha production in macrophages. Blood 2003; 102:4123–4129
44. Riemann M, Endres R, Liptay S, Pfeffer K, Schmid RM. The IkappaB protein Bcl-3 negatively regulates transcription of the IL-10 gene in macrophages. J Immunol 2005;175:3560–3568
45. Totzke G, Essmann F, Pohlmann S, Lindenblatt C, Jänicke RU, Schulze-Osthoff K. A novel member of the IkappaB family, human IkappaB-zeta, inhibits transactivation of p65 and its DNA binding. J Biol Chem 2006;281: 12645–12654
46. Yamazaki S, Muta T, Takeshige K. A novel IkappaB protein, IkappaB-zeta, induced by proinflammatory stimuli, negatively regulates nuclear factor-kappaB in the nuclei. J Biol Chem 2001;276:27657–27662
47. Zhong H, May MJ, Jimi E, Ghosh S. The phosphorylation status of nuclear NF-kappa B determines its association with CBP/p300 or HDAC-1. Mol Cell 2002;9:625–636
48. Albers JW, Herman WH, Pop-Busui R, et al.; Diabetes Control and Complications Trial/Epidemiology of Diabetes Interventions and Complications Research Group. Effect of prior intensive insulin treatment during the Diabetes Control and Complications Trial (DCCT) on peripheral neuropathy in type 1 diabetes during the Epidemiology of Diabetes Interventions and Complications (EDIC) Study. Diabetes Care 2010;33:1090–1096
49. Launer LJ, Miller ME, Williamson JD, et al.; ACCORD MIND investigators. Effects of intensive glucose lowering on brain structure and function in people with type 2 diabetes (ACCORD MIND): a randomised open-label substudy. Lancet Neurol 2011;10:969–977